BRITISH GEOLOGICAL SURVEY
Natural Environmental Research Council

Fluid Processes & Waste Management Series

Technical Report WE/98/12R

Stress-sensitivity of the hydraulic properties of a clay-bearing fault gouge from the Tsukiyoshi Fault, Tono Mine, Central Japan

by

J.F. Harrington and S.T. Horseman

Transport Properties Research Laboratory

A report prepared for the
Japan Nuclear Cycle Development Institute (JNC)

The opinions and conclusions of this report are those of the authors and do not necessarily represent those of the funding agency.

Keyworth, Nottingham (UK)

Tel: +44 (0) 115 9363100
Fax: +44 (0) 115 9363261

EXECUTIVE SUMMARY

The scope of the work commissioned by JNC (Japan) and described in this report was to conduct a series of laboratory experiments on a single specimen of clay-bearing fault gouge to provide information on hydraulic properties and the sensitivity of these properties to isotropic confining stress. The specimen was prepared so that the direction of flow was perpendicular to the strike of the fault and roughly horizontal. The tests therefore relate to the transverse hydraulic conductivity of the fault zone. Controlled flow-rate experiments were performed at three levels of isotropic confining stress with a fixed backpressure. Hydraulic conductivities were calculated from steady-state pressure gradients and from analysis of the pressure transients. Transient analysis also yielded values for specific storage.

At confining stresses of 3.5, 7.5 and 13.5 MPa the average hydraulic conductivities based on analysis of steady-state pressure gradients were 1.84×10^{-12} m.s^{-1}, 1.79×10^{-13} m.s^{-1} and 7.9×10^{-14} m.s^{-1}. The equivalent values from analysis of the pressure transients were 2.09×10^{-12} m.s^{-1}, 2.06×10^{-13} m.s^{-1} and 8.4×10^{-14} m.s^{-1}. Hydraulic conductivity is strongly-dependent on the spherical component of the effective stress tensor.

Given the crumbly and poorly-cohesive matrix of this material, the presence of significant amounts of sand-sized material, and the occurrence of shear-induced features (e.g. slickenslides), the fault gouge has exceptionally low hydraulic conductivity.

Based on these experiments, the transverse hydraulic conductivity of the clay-bearing fault gouge at the sampling depth of 160 m in the North Extension Drift is around 2×10^{-12} m.s^{-1}. Extrapolation of the experimental data suggests that hydraulic conductivity increases at shallower depths, with a value of around 1×10^{-11} m.s^{-1} at the surface. Although it is not possible to comment on the effects of scale and heterogeneity, it would appear that the clay-bearing component of the fault gouge has much lower hydraulic conductivity than the surrounding country rocks.

The experiments indicate that the Tsukiyoshi Fault gouge behaves as an overconsolidated material. The material is therefore in a much denser state of packing than one would anticipate from current effective stress. The combined effects of prior consolidation under high spherical effective stress and high deviatoric (shear) stress may explain the very low hydraulic conductivity of this material. Estimates for the recent burial history of the formation indicate that approximately 500 m of overburden have been removed by erosion, which would account for the overconsolidated nature of the Tsukiyoshi Fault gouge.

Specific storage can be written in terms of the drained bulk modulus of the material and the bulk modulus of water and can be predicted from the soil mechanics κ (kappa) parameter. The derived theoretical relationship is in reasonable agreement with experimental data for effective stresses greater than 4 MPa, but is inadequate in the low stress regime. At the sampling depth in the North Extension Drift, the specific storage of the clay-bearing fault gouge is around 7.5×10^{-5} m^{-1}. Specific storage increases at shallower depths.

Recommendations are made for additional laboratory studies of the mineralogy, fabric and fluid flow properties of the fault gouge.

CONTENTS PAGE

1 INTRODUCTION

Tono Mine is located about 350 km southwest of Tokyo and is the site of Japan s most extensive uranium deposits. The geological setting comprises Tertiary (Mizunami Group) sedimentary rocks overlying Cretaceous granitic basin. In ascending order, the sedimentary rocks are the Toki Lignite-bearing Formation (conglomerate, interbedded sandstone and mudstone), the Akeyo Formation (tuffaceous sandstone) and the Oidawara Formation (siltstone and mudstone). The Tsukiyoshi Fault cuts through this sequence and is a reverse fault, dipping to the south at 60-70 degrees, with a throw of about 30 metres (Koide et al., 1998).

As part of its hydrogeological studies, PNC is evaluating the impact of the Tsukiyoshi Fault on groundwater flow in the Tertiary sediments. The construction of a new shaft provided an opportunity to study draw-down effects. A series of boreholes were instrumented with multiple piezometers allowing transient hydraulic heads to be monitored during shaft excavation. Comparison of head responses on either side of the fault allowed inferences to be made on the hydraulic properties of the fault (Koide et al., 1998).

In the No. 2 Measurement Drift, the hanging wall of the fault (upthrow side) comprises the conglomerate of the Toki Lignite-bearing Formation and the footwall (downthrow side) comprises the tuffaceous sandstone of the Akeyo Formation. The fault zone consists of gouge material with two clay-bearing layers around 2-3 cm thick, separated by a 10-20°cm thick layer of unconsolidated fine sandy material.

1.1 Scope of work

The scope of the work described in the report was to conduct a series of laboratory experiments on a single specimen of clay-bearing fault gouge to provide information on hydraulic properties and the sensitivity of these properties to isotropic confining stress (i.e. the spherical component of the stress tensor). The specimen was prepared so that the direction of flow was perpendicular to the strike of the fault and roughly horizontal. The tests therefore relate to the transverse hydraulic conductivity of the fault zone.

Controlled flow-rate experiments were performed at three levels of isotropic confining stress with a fixed backpressure. Hydraulic conductivities were calculated from steady-state pressure gradients and from analysis of the pressure transients. Transient analysis also yielded values for specific storage.

1.2 Description of test material

Sampling of the fault gouge material was undertaken in July 1997. A 116 mm diameter sub-horizontal borehole was drilled using a Koken OE-8 rotary drilling machine at a location in the North Extension Drift of Tono Mine, approximately 160 metres below surface. The borehole was inclined at an angle of 5 degrees below horizontal and the total length was 29.96 m. The sample was obtained using a triple-tube core barrel fitted with a split sample tube and a diamond bit. The hole was water-flushed using local river water. In total, 15 cm of clay-bearing fault gouge material was recovered. This was substantially more than the reported exposure in No. 2 Measurement Drift. The sample was trimmed to length, then vacuum sealed in double aluminised plastic bags which were flushed with nitrogen prior to sealing. The sample was carefully packed in a wooden transit box and shipped to the United Kingdom.

On receipt, the sample was examined by a geologist. Photographs and sketches were prepared. The sample comprised a crumbly and poorly-cohesive matrix of olive-green/grey gouge material with particles ranging from clay-size through to sand-size

(i.e. poorly-sorted in sedimementological terms), containing conspicuous white crystals of a soft, friable and altered mineral, possibly calcite (Figure 1). Data supplied by JNC show the green colour is due to the presence of the clay mineral chlorite. The sample had a strongly-sheared fabric and was cut by numerous shiny shear surfaces (slickensides) with a grey-brown colouration suggestive of chemical alteration. These so-called listric surfaces appeared to be regions of clay mineral re-orientation with the basal surfaces of clay platelets lying in the plane of shear deformation. This mineral alignment was apparent even at the fine scale, with platy clay minerals draped around inclusions forming Augen-like structures.

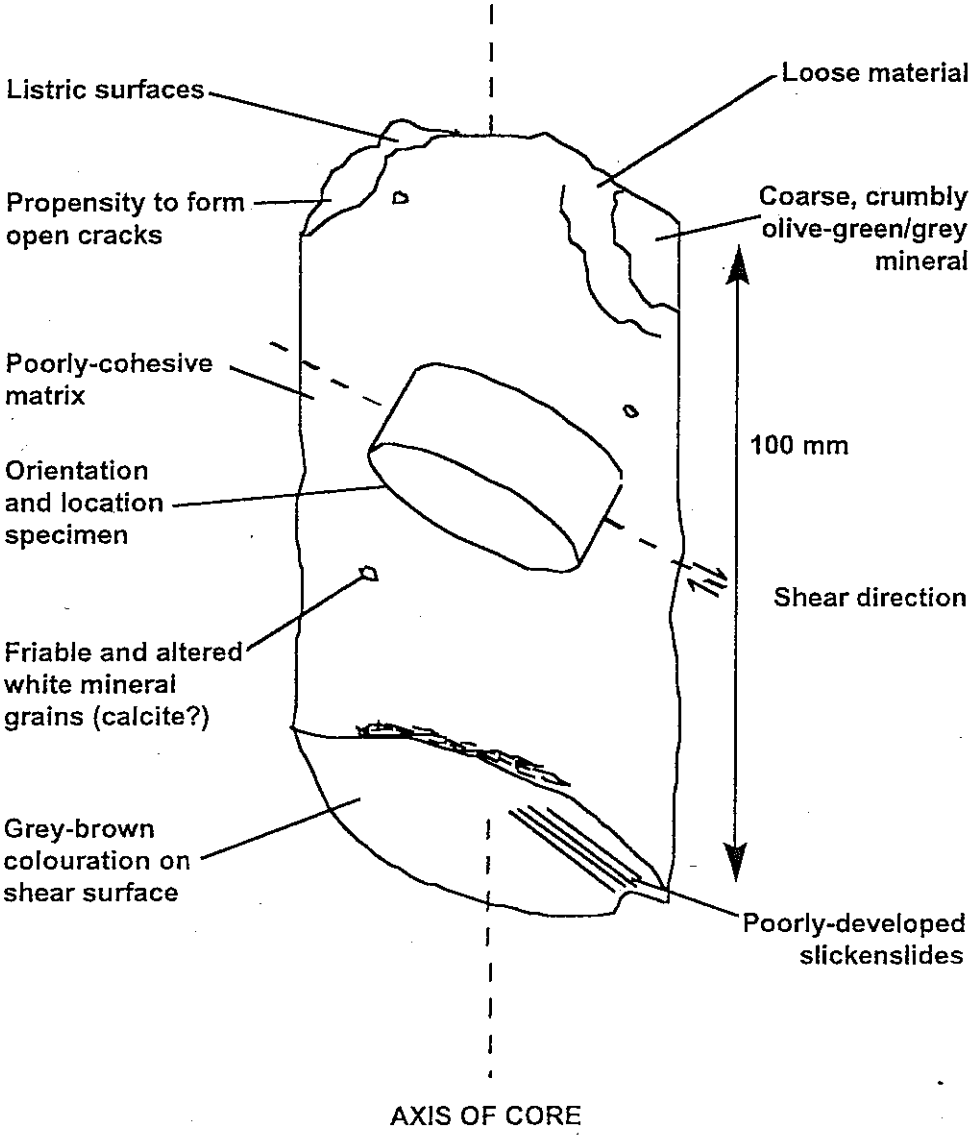

Figure 1 Sketch of sample showing location of test specimen

2 EXPERIMENTAL DETAILS

The BGS controlled flow rate permeameter (Figure 2) consists of five main components: (1) a sample assembly, (2) a 40 MPa-rated pressure vessel and associated confining pressure system, (3) a fluid injection system, (4) a backpressure system and (5) a microcomputer-based data acquisition system. The sample is subject to an isotropic confining stress.

2.1 Pressure vessel and sample assembly

The pressure vessel, shown in Figure 3, comprises a cylindrical Autoclave Engineers bolted single-closure reactor vessel, made from 316 stainless steel. The specimen is 4.90 cm in diameter with a length of 2.54 cm. It is sandwiched between two end-caps, each with a 316 sintered stainless steel porous disc, and jacketed in heat-shrink Teflon to exclude confining fluid and provide a flexible pressure seal.

2.2 Injection, backpressure and confining pressure circuits

The ingoing volumetric flow rate and backpressure are controlled using a pair of ISCO-100, Series D, syringe pumps operated from a single digital control unit. A pressure transducer monitors outgoing pressure to provide a feedback signal to the microprocessor when each pump is set to constant pressure mode. Piston motion then gives a direct measure of the net volumetric flow out of each pump. The pumps can also be set to constant volumetric pumping rate, whereby the piston is advanced at a constant velocity. Confining pressure is maintained using compressed nitrogen.

2.3 Instrumentation and data acquisition

The ISCO pump controller has an RS232 serial port which allows volume, flow rate and pressure data to be transmitted to an equivalent port on a 32-bit personal computer. A programme written in QBASIC prompts the pump controller to transmit data to the computer at pre-set time intervals. Acquisition rate was one scan per 30 minutes.

2.4 Calibration

Both ISCO syringe pumps were pressure calibrated using a Druck PTX610 transmitter. Steps of 1.0 MPa in pressure were applied, with increments and decrements to quantify hysteresis. Using a spreadsheet, least-squares regression fits were calculated and the parameters used to correct the raw data.

2.5 Sample preparation

The sample was manufactured in the normal manner using a former with a sharpened leading edge. Excess material was trimmed away using a scalpel. The upper and lower surfaces were finished-off using a scraping action with a flat-bladed knife, leaving the end-surfaces flat and parallel. Purite-saturated[1] sintered discs were placed on each face of the specimen, the end-caps were positioned, and the resulting assembly jacketed in Teflon heat-shrink tube. The jacket was shrunk to size using a hot air gun. Two hose clamps were tightened onto copper shims to compress the Teflon on to the end-caps, resulting in a leak-tight seal. Tubing connections were then made to the vessel end-closure (Figure 3).

2.6 Basic physical properties

Table 1 shows the basic physical properties of the test sample based on pre-test measurements of water content[2] and an assumed specific gravity for the mineral solids. The prepared specimen was found to be slightly desaturated under atmospheric conditions (degree of saturation = 86.8%).

[1] Purite is a commercial name for double-distilled water.
[2] Water content was determined by oven drying at 105°C for a period in excess of 24 hours.

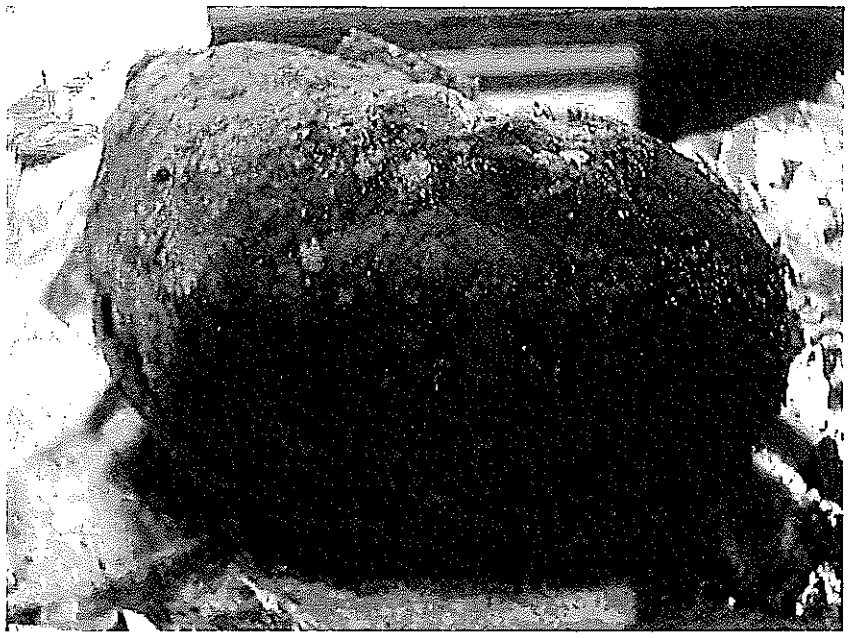

Plate 1 **Sample TFA-1 after removal from the aluminised plastic wrapping**

Plate 2 **Sample TFA-1 showing the crumbly, poorly-cohesive nature of the gouge material. The olive-green/grey colouration is due to the presence of the clay mineral (chlorite).**

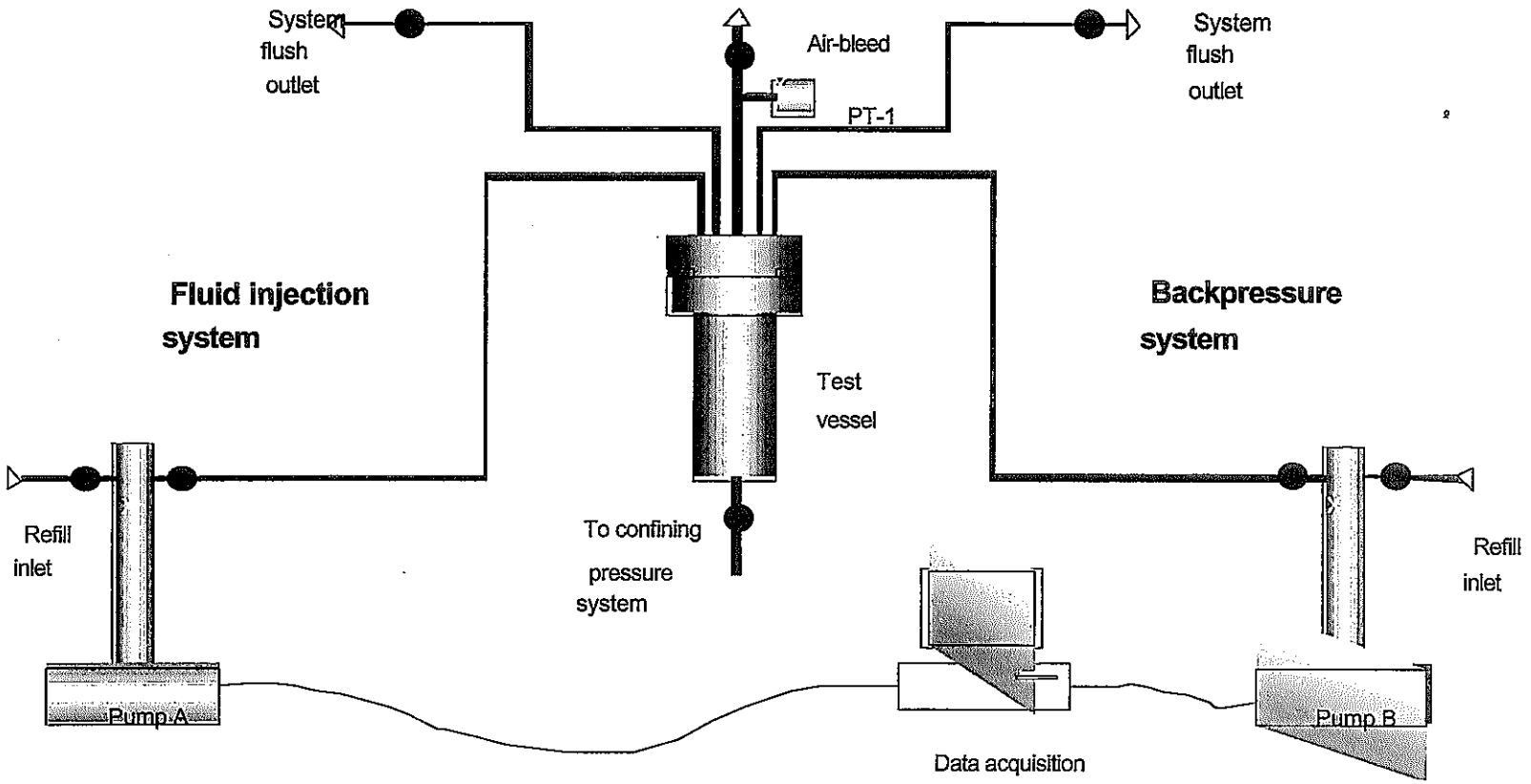

Figure 2 Schematic of test apparatus

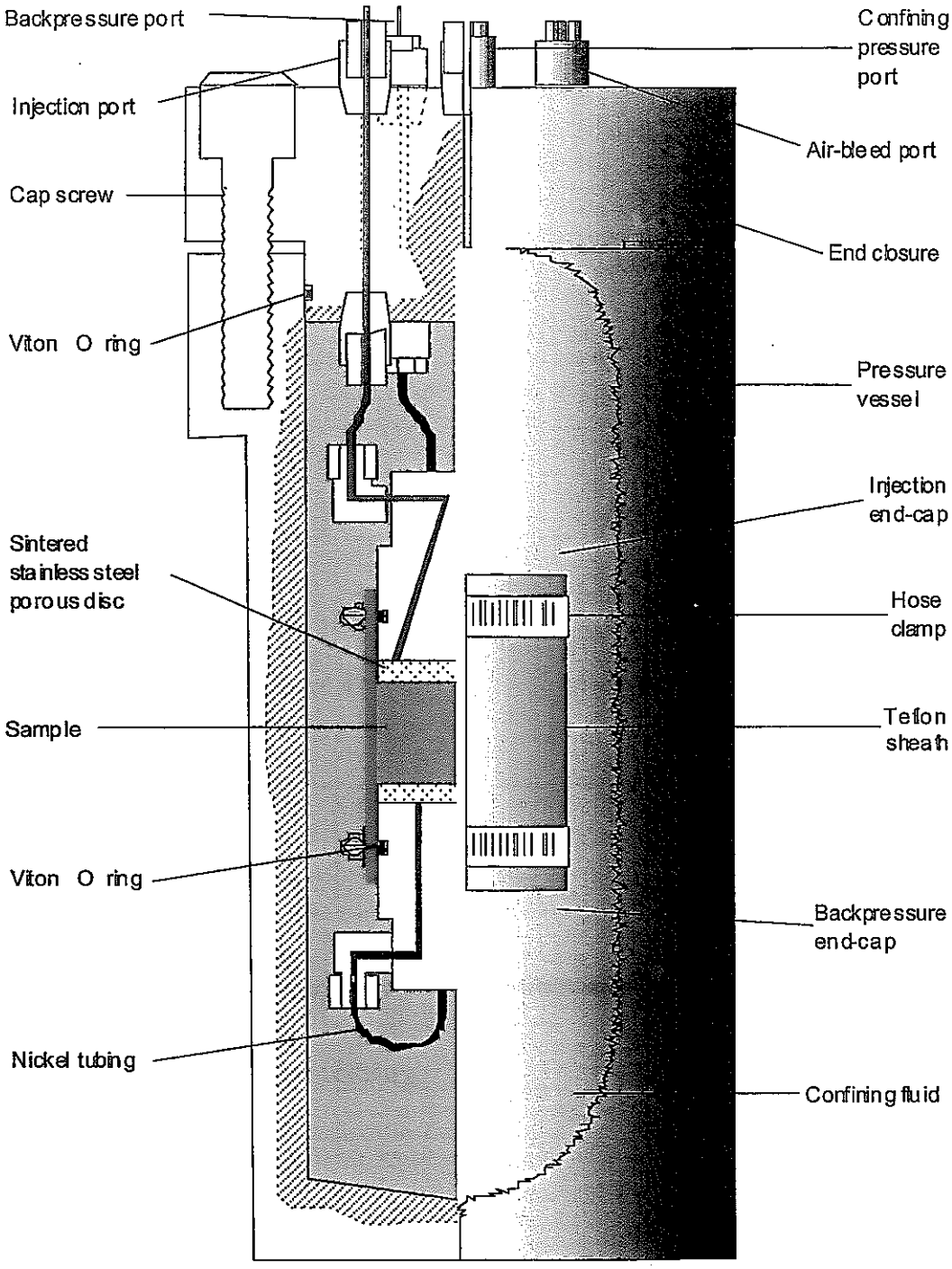

Figure 3 **Schematic of pressure vessel and sample assembly**

Sample number	Sampling interval (m)	Water content (wt-%)	Bulk density ($Mg.m^{-3}$)	Dry density ($Mg.m^{-3}$)	Void ratio	Porosity	Degree of saturation
TFA-1	14.60-14.79	15.3	2.10	1.82	0.475	0.32	0.868

Table 1 Basic physical properties of the test specimen from pre-test measurements of water content assuming an average specific gravity for the mineral phases of 2.69 $Mg.m^{-3}$. The sampling interval is relative to driller s datum.

Previous work has shown that it is very important to correct the degree of saturation and other dependent properties for the effect of applying the confining stress to the material. Assuming ideal gas behaviour and no dissolution of gas in porewater, the relationship between the void ratio of a compressible clay-like material and the saturation S_w^{at} under atmospheric conditions and the void ratio of the same material under confinement e^{tc}, can be estimated using

$$e^{tc} = e^{at}\left(S_w^{at}\right) + e^{at}\left(1 - S_w^{at}\right)R_p \qquad (1)$$

where R_p is the ratio of atmospheric pressure (0.1 MPa) to the air pressure in the sample when subjected to confinement. This ratio is likely to be around 0.03 for the lowest value of confining stress used in these experiments. The degree of saturation of the confined specimen becomes

$$S_r^{tc} = \frac{wG_s}{e^{at}\left(S_w^{at}\right) + e^{at}\left(1 - S_w^{at}\right)R_p} \qquad (2)$$

where w is the gravimetric water content and G_s is the average specific gravity of the mineral solids. Under experimental conditions, void ratio falls to around 0.414 and the degree of saturation rises very close to unity (Table 2). Any residual gas left within the specimen probably enters solution, a process assisted by the use of vacuum de-aired Purite.

Sample number	Sampling interval (m)	Water content (wt-%)	Bulk density ($Mg.m^{-3}$)	Dry density ($Mg.m^{-3}$)	Void ratio	Porosity	Degree of saturation
TFA-1	14.60-14.79	15.3	2.19	1.90	0.414	0.29	0.996

Table 2 **Basic physical properties of the test sample corrected for the effects of confining pressure on degree of saturation using Equations (1) and (2).**

2.7 Stress conditions for testing

Taking the vertical total stress gradient in the region of Tono Mine as 0.022 $MPa.m^{-1}$, the undisturbed vertical stress in the fault zone at 160 m below surface is 3.5 MPa. Assuming the hydrostatic pressure of water at this depth to be around 1.5 MPa, the vertical effective stress on the fault gouge would be 2 MPa. The test programme was scheduled to include controlled flow rate (CFR) stages at an effective stress close to 2 MPa.

2.8 Experimental history

Table 3 shows the experimental history. During an equilibrium (EQ) stage the specimen is backpressured with Purite on both faces (i.e. zero hydraulic gradient). The purpose of this stage is to allow excess pore pressures to dissipate. A controlled flow rate (CFR) stage is used to evaluate hydraulic conductivity and specific storage and involves the injection of Purite into the specimen at volumetric flow rates shown in Table 3.

Stage No.	Type	Flow rate ($\mu L.hr^{-1}$)	Confining pressure (MPa)	Back-pressure (MPa)	Effective stress (MPa)
1	EQ	-	3.50	1.51	1.99
2	CFR	10	3.50	1.51	-
3	CFR	20	3.50	1.51	-
4	CFR	30	3.50	1.51	-
5	CFR	20	3.50	1.51	-
6	CFR	10	3.50	1.51	-
7	EQ	-	3.50	1.51	1.99
8	EQ	-	7.50	1.51	5.99
9	CFR	10	7.50	1.51	-
10	CFR	15	7.50	1.51	-
11	CFR	20	7.50	1.51	-
12	CFR	15	7.50	1.51	-
13	CFR	10	7.50	1.51	-
14	EQ	-	7.50	1.51	5.99
15	EQ	-	13.50	1.51	11.99
16	CFR	5	13.50	1.51	-
17	CFR	10	13.50	1.51	-
18	CFR	15	13.50	1.51	-
19	CFR	10	13.50	1.51	-
20	CFR	5	13.50	1.51	-
21	EQ	-	13.50	1.51	11.99

Table 3 stage **Summary of experimental history showing stage numbers, type of (EQ = equilibration, and CFR = conntrolled flow rate), flow rate, confining pressure (MPa), backpressure (MPa) and effective stress (MPa).**

3 DATA REDUCTION

Data were transferred to a spreadsheet for processing and plotting. Hydraulic transients were very well-defined and largely free of experimental noise.

The one-dimensional equation of flow is

$$S_s \frac{\partial h}{\partial t} = K \frac{\partial^2 h}{\partial x^2} \qquad (3).$$

where S_s (m^{-1}) is the specific storage, K ($m.s^{-1}$) is the hydraulic conductivity, h (m) is the hydraulic head and x (m) is distance in the flow direction. This equation must be solved subject to the boundary conditions

$$q = \frac{Q}{A_s} = -K \left. \frac{\partial h}{\partial x} \right|_{x=0} \qquad (4)$$

and

$$h = 0 \text{ at } x = L_s \qquad (5)$$

where q ($m.s^{-1}$) is the Darcy velocity, Q ($m^3.s^{-1}$) is the volumetric flow rate, A_s (m^2) and L_s (m) are the cross-sectional area and length of the specimen, respectively. Hydraulic head is related to the pore pressure, P (Pa), by

$$h = \frac{P}{\rho_w g} \qquad (6)$$

where ρ_w ($kg.m^{-3}$) is the density of water and g (= 9.81 $m.s^{-2}$) is the acceleration due to gravity.

The head at x = 0 as a function of time was obtained by numerically inverting the Laplace Transform solution given in Appendix 1. Five parameters are required to define the solution. Three are experimentally determined: Q, A_s, and L_s. The remaining two are the material properties that the test is designed to determine (i.e. K and S_s). In order to estimate the values of these parameters, a general nonlinear least squares fitting routine was used to minimise the differences between the calculated curves and the measured head data.

Hydraulic conductivity was also calculated from the head gradient at steady-state enabling the two values to be compared.

Permeability, k (m^2), was calculated from hydraulic conductivity using the relationship

$$k = \frac{K\eta_w}{\rho_w g} \qquad (7)$$

where η_w (Pa.s) is the viscosity of water.

Volumetric strains and instantaneous values of void ratio were obtained from the difference between the volume pumped in and the volume pumped out of the specimen. No correction was applied for compression of the pump barrel, piston, seals and liquid phase.

4 RESULTS

Figure 4 shows a typical consolidation curve for an equilibrium (EQ) stage. The cumulative flow out of the specimen is plotted against the square root of time in the usual manner. Figures 5 to 19 show the hydraulic transients following changes in flow rate for the controlled flow rate (CFR) stages. The least square fits to the data are shown in red and clearly provide a very good representation of the transient responses. Summarised results are presented in Table 4. Overall, the experiments were highly successful and provide a very consistent data set for this gouge material.

4.1 Adequacy of Darcy s Law

For each level of confining stress, the hydraulic conductivity values are fairly constant over the ranger of flow rates. This is evidence for the general validity of Darcy s Law for this material. However, close inspection of the data reveals a degree of flow-rate sensitivity accompanied by some hysteresis. This can be partially explained by the dependence of hydraulic conductivity on effective stress (Section 4.4). As flow rate increases, the average pore pressure in the test specimen also increases. Under a fixed confining stress, an increase in pore pressure signifies a decrease in effective stress. This decrease in effective stress causes the small change in hydraulic conductivity, leading to the apparent flow-rate sensitivity of this parameter.

Stage No.	Average effective stress (MPa)	From steady-state pressure		From transient analysis		Specific storage S_s / 10^{5} (m^{-1})
		Hydraulic conductivity K / 10^{12} ($m.s^{-1}$)	Permeability k / 10^{19} (m^2)	Hydraulic conductivity K / 10^{12} ($m.s^{-1}$)	Permeability k / 10^{19} (m^2)	
Isotropic confining stress = 3.5 MPa						
2	1.89	1.81	1.85	1.80	1.84	5.19
3	1.79	1.85	1.89	2.12	2.17	8.57
4	1.70	1.88	1.92	2.19	2.34	9.68
5	1.78	1.80	1.83	2.02	2.06	5.93
6	1.89	1.84	1.88	2.08	2.13	8.32
AVERAGE		**1.84**	**1.88**	**2.04**	**2.09**	**7.54**
Isotropic confining stress = 7.5 MPa						
9	4.91	0.171	0.174	0.173	0.177	3.78
10	4.44	0.178	0.182	0.206	0.210	5.12
11	4.03	0.187	0.191	0.224	0.229	4.86
12	4.45	0.179	0.183	0.222	0.227	4.46
13*	5.37	0.298	0.304	0.094	0.096	6.08
AVERAGE		**0.179**	**0.182**	**0.206**	**0.211**	**4.56**
Isotropic confining stress = 13.5 MPa						
16	10.76	0.075	0.076	0.076	0.078	3.08
17	9.65	0.078	0.080	0.082	0.084	3.27
18	8.66	0.083	0.084	0.090	0.092	3.61
19	9.69	0.080	0.081	0.090	0.092	2.98
20	10.82	0.078	0.080	0.082	0.084	3.21
AVERAGE		**0.079**	**0.080**	**0.084**	**0.086**	**3.23**

Table 4 Hydraulic properties of clay-bearing gouge material from the Tsukiyoshi Fault, showing stage number, average effective stress, hydraulic conductivity and permeability (based on controlled flow rate tests), transient hydraulic conductivity, permeability and specific storage (based on analysis of the transient pore pressure responses). Test stage indicated by * is considered unrepresentative and values are omitted from the averages.

4.2 Comparison between methods of obtaining hydraulic conductivity

At a confining stress of 3.5 MPa the average hydraulic conductivity from analysis of steady-state pressure gradients is 1.84 x10^{-12} $m.s^{-1}$. The equivalent value from analysis of the pressure transients is 2.09 x10^{-12} $m.s^{-1}$.

At a confining stress of 7.5 MPa the average hydraulic conductivity from analysis of steady-state pressure gradients is 1.79 x10^{-13} $m.s^{-1}$. The equivalent value from analysis of the pressure transients is 2.06 x10^{-13} $m.s^{-1}$.

At a confining stress of 13.5 MPa the average hydraulic conductivity from analysis of steady-state pressure gradients is 7.9 x10^{-14} $m.s^{-1}$. The equivalent value from analysis of the pressure transients is 8.4 x10^{-14} $m.s^{-1}$.

Apparently, the hydraulic conductivity from steady-state pressure gradients is always a little smaller (87 to 94%) than the value derived by analysis of the transient response. Inspection of Table 4 shows that hydraulic conductivity from transient analysis is more sensitive to flow rate (and effective stress) than hydraulic conductivity from steady-state pressure gradients. Theses differences are reflected in the averages.

4.3 Volume changes during testing

The void ratio, e, of the gouge material is defined as the ratio of the volume of voids to the total volume of the sample. It is related to porosity, n, by

$$n = \frac{e}{1+e} \tag{8}$$

Figure 20 shows the standard soil mechanics plot of void ratio against the logarithm of effective stress. The blue curve represents the behaviour of the sample when the confining stress is increased and backpressure held constant. In soil mechanics terms, this curve is known as the rebound-reconsolidation line (RRL). It is sensibly linear in the log-linear parameter space, and can be represented by the expression

$$e = e_o - \kappa \ln\left(\frac{\sigma'}{\sigma_0'}\right) \tag{9}$$

where $-\kappa$ is the slope of the RRL, σ is the effective stress acting on the specimen, e_0 is the void ratio intercept at an effective stress σ_0 = 1.0 MPa (Schofield and Wroth, 1968). For effective stresses in the range 2 to 6 MPa, κ = 0.036 and e_0 = 0.4385. For effective stresses in the range 6 to 12 MPa, κ increases to 0.044.

The data shown in red represent the volumetric behaviour of the specimen during the CFR test stages. For effective stresses greater than 4 MPa, the volumetric behaviour for an increasing history of flow rate corresponds fairly closely with the RRL. This provides good confirmation that the fault gouge is overconsolidated (Atkinson and Bransby, 1978). For a decreasing history of flow rate, the path in e-ln(σ) space is less steep than the RRL. For effective stresses around 2 MPa, both paths are less steep than the RRL.

4.4 Sensitivity of hydraulic conductivity to stress

Figure 21 is a plot of hydraulic conductivity against average effective stress. Extrapolation gives a value of around 1 x10^{-11} m.s^{-1} at zero effective stress. Based on this trend, hydraulic conductivity changes most rapidly between zero and 5.0 MPa. Beyond 5.0 MPa hydraulic conductivity becomes less sensitive to changes in effective stress. One possible interpretation is that the fault gouge is clay matrix-supported at stress less than 5.0 MPa and is framework-supported at higher stresses. However, the measured increase in κ with stress is not consistent with this hypothesis.

4.5 Sensitivity of specific storage to stress

According to Horseman et al. (1996, p173), the drained bulk modulus, B, of an overconsolidated clay can be expressed as a function of void ratio and effective stress as follows

$$B = \frac{(1+e)\sigma'}{\kappa} \tag{10}$$

The specific storage of the material is given by

$$S_s = \rho_w g\left[\frac{1}{B} + \frac{n}{B_w}\right] \qquad (11)$$

where n is the porosity and B_w (= 2.2 GPa) is the bulk modulus of water. Combining (8), (10) and (11) gives the relationship:

$$S_s = \frac{\rho_w g}{1+e}\left[\frac{\kappa}{\sigma'} + \frac{e}{B_w}\right] \qquad (12)$$

Specific storage therefore depends on two variables, the current void ratio and the effective stress. Figure 22 shows experimentally-determined values for specific storage, together with this theoretical relationship (assuming κ = 0.036). The theoretical curve is less satisfactory at low values of effective stress. This can be explained by the discrepancy between the slopes of the paths in e-ln(σ) space during CFR testing at low effective stress and the slope of the RRL (Figure 20).

5 CONCLUSIONS

The experiments were highly successful and have provided a very consistent data set for this clay-bearing gouge material from the Tsukiyoshi Fault.

Given the crumbly and poorly-cohesive matrix of this material, the presence of significant amounts of sand-sized material, and the occurrence of shear-induced features (e.g. slickenslides), the fault gouge has exceptionally low hydraulic conductivity.

The specimen was prepared so that the direction of flow was perpendicular to the strike of the fault and roughly horizontal (i.e. the tests relate to the transverse hydraulic conductivity of the fault zone).

At confining stresses of 3.5, 7.5 and 13.5 MPa the average hydraulic conductivities based on analysis of steady-state pressure gradients were 1.84 x10^{-12} m.s^{-1}, 1.79 x10^{-13} m.s^{-1} and 7.9 x10^{-14} m.s^{-1}. The equivalent values from analysis of the pressure transients were 2.09 x10^{-12} m.s^{-1}, 2.06 x10^{-13} m.s^{-1} and 8.4 x10^{-14} m.s^{-1}. Hydraulic conductivity is strongly-dependent on the spherical component of the effective stress tensor. Beyond 5 MPa, hydraulic conductivity becomes less sensitive to effective stress. One possible interpretation is that the fault gouge is clay matrix-supported at low stress and framework-supported at high stress. In other words, the coarser particles may lock together at high stress, sheltering the fine-grained component from the full effect of the applied stress.

The hydraulic conductivity from steady-state pressure gradients is always a little smaller (87 to 94%) than the value derived by analysis of the transient response. For each level of confining stress, the hydraulic conductivity values are fairly constant over the range of flow rates. This is evidence for the general validity of Darcy s Law for this material. However, close inspection of the data reveals a degree of flow-rate sensitivity accompanied by some hysteresis. This can be partly explained by the dependence of hydraulic conductivity on effective stress.

Based on these experiments, the transverse hydraulic conductivity of the clay-bearing fault gouge at a the sampling depth of 160 m in the North Extension Drift is around 2 x10^{-12} m.s^{-1} (i.e. roughly equivalent to the hydraulic conductivity to the Boom Clay at the depth interval of the Hades URL in Belgium). Extrapolation of the experimental data suggests that hydraulic conductivity increases at shallower depths, with a value of around 1 x10^{-11} m.s^{-1} at the surface. Although it is not possible to comment on the effects of scale and heterogeneity, it would appear that the clay-bearing component of the fault gouge has much lower hydraulic conductivity than the surrounding country rocks.

in e-ln(σ) space corresponds to the rebound-reconsolidation line (RRL) of theoretical soil mechanics. The slope of this line, -κ, has a value of around 0.036, increasing to 0.044 at effective stresses greater than 6 MPa.

These observations show that Tsukiyoshi Fault gouge behaves as an overconsolidated material (Atkinson and Bransby, 1978). In effect, the current effective stress on this material is substantially less than the effective stress during faulting. The material is therefore in a much denser state of packing than one would anticipate from current effective stress. The combined effects of prior consolidation under high spherical effective stress and high deviatoric (shear) stress may explain the very low hydraulic conductivity of this material.

Estimates for the recent burial history of the formation indicate that around 600 m of overburden have been removed by erosion. Since the fault gouge is overconsolidated, it indicates that faulting occurred prior to geological exhumation. This estimate for geological uplift (500 m) is in line with the geotechnical data which indicates that the fault gouge is still overconsolidated and on the same RRL at a stress equivalent to a depth of burial of 550 m ($\approx$12 MPa).

For effective stresses greater than 4 MPa, the volumetric behaviour for an increasing history of flow rate corresponds fairly closely with the RRL. Specific storage can be written in terms of the drained bulk modulus of the material and the bulk modulus of water. Since the drained bulk modulus depends on the slope of the RRL, it is possible to predict specific storage from soil mechanics parameters. The derived theoretical relationship is in reasonable agreement with experimental data for effective stresses greater than 4 MPa, but is inadequate in the low stress regime.

At the sampling depth in the North Extension Drift, the specific storage of the clay-bearing fault gouge is around 7.5 x10^{-5} m^{-1}. Specific storage increases at shallower depths.

6 RECOMMENDATIONS

Given that laboratory experiments are now proven to provide very useful results, we strongly recommend that more samples be tested in this way to provide information on spatial variability and possible anisotropy of hydraulic properties. The study has focused on the role of the spherical component of the stress tensor additional work might also be performed on deviatoric (shear) component. We recommend that all test samples are analysed for mineralogy, fabric (SEM studies), specific surface and particle and pore size distributions. Furthermore, all cores from the Tsukiyoshi Fault should be logged by a competent structural geologist with the aim of recording all features linked to fault movement. As a final recommendation, we suggest that gas breakthrough pressures and gas permeabilities be measured to assist in generic studies of repository gas migration.

RFERENCES

Atkinson, J.H. and P.L. Bransby (1978). The Mechanics of Soils: An Introduction to Critical State Soil Mechanics. McGraw-Hill, New York.

Horseman, S.T., J.J.W. Higgo, J. Alexander and J.F. Harrington (1996). Water, gas and solute movement through argillaceous media. A report prepared for the OECD/NEA Working Group on Measurement and Physical Understanding of Groundwater Flow Through Argillaceous Media (Clay Club), prepared by Fluid Processes Group, British Geological Survey, Nottingham, UK, Rept CC-96/1, OECD Paris, 290pp.

Koide, K., M. Yamane and K. Kobayashi (1998). Heterogeneity of hydraulic conductivity of a fault in sedimentary sequences at the Tono Mine, Central Japan. In: Proceedings of a joint NEA/EC Workshop on Fluid Flow through Faults and Fractures in Argillaceous Formations, Berne, Switzerland, 10-12 June 1996, 189-198.

Schofield, A. and P.W. Wroth (1968). Critical State Soil Mechanics, McGraw-Hill, London.

Talbot, A. (1979). The accurate numerical inversion of Laplace Transforms. J. Inst. Math. Applications, (23), 97.

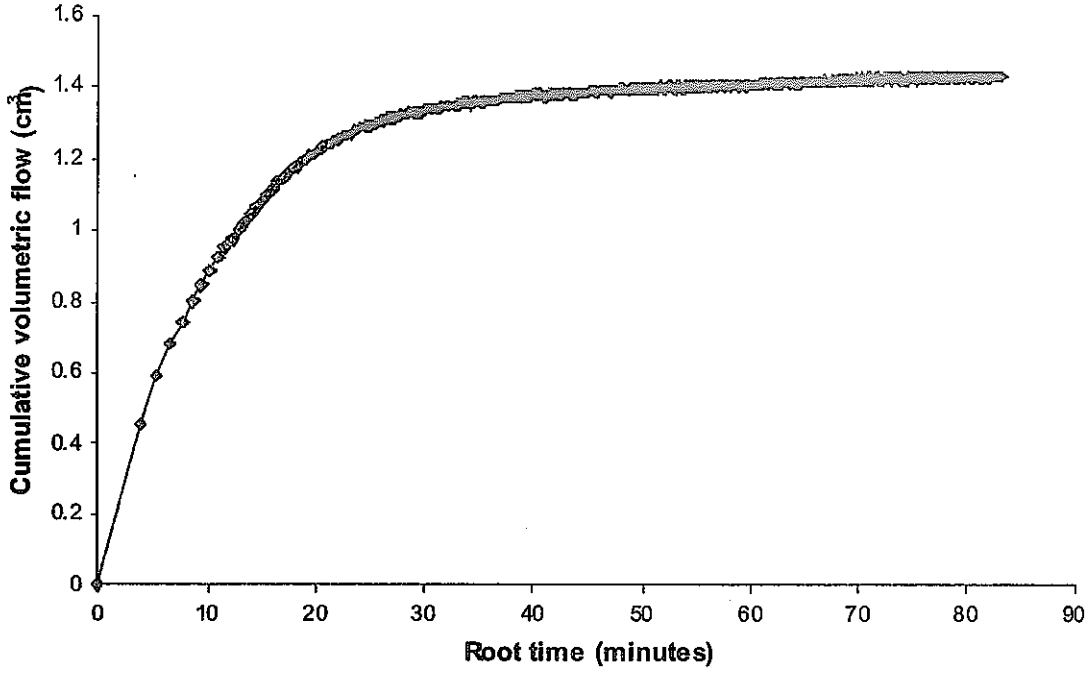

Figure 4 **Typical consolidation curve (EQ —Stage 8)**

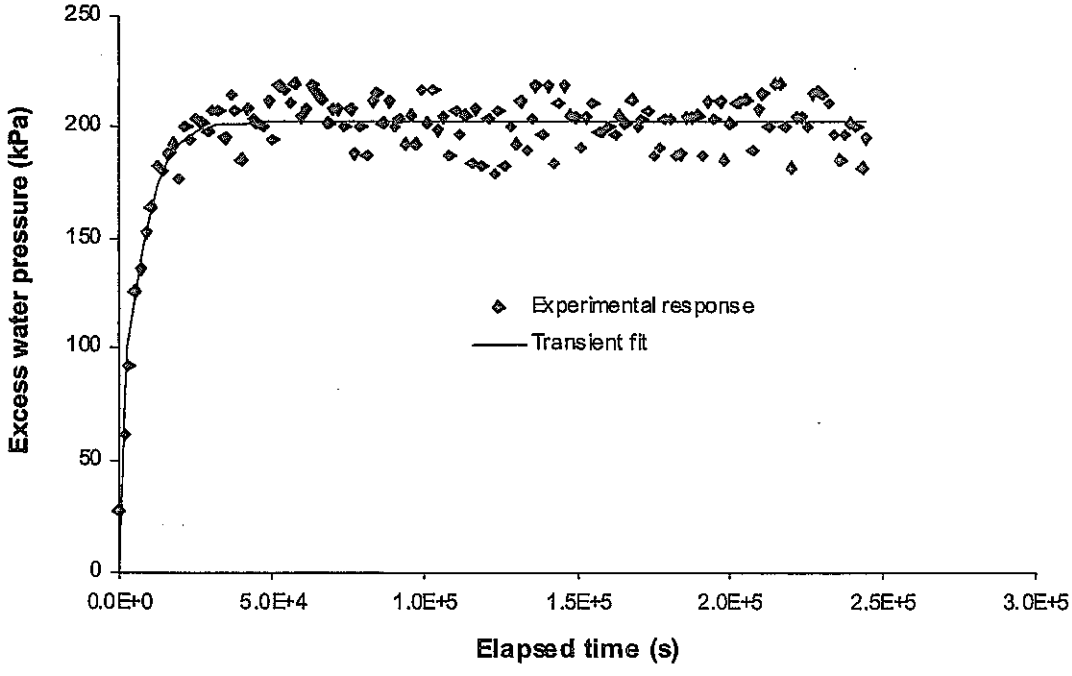

Figure 5 **Transient analysis of excess water pressure (stage 2)**

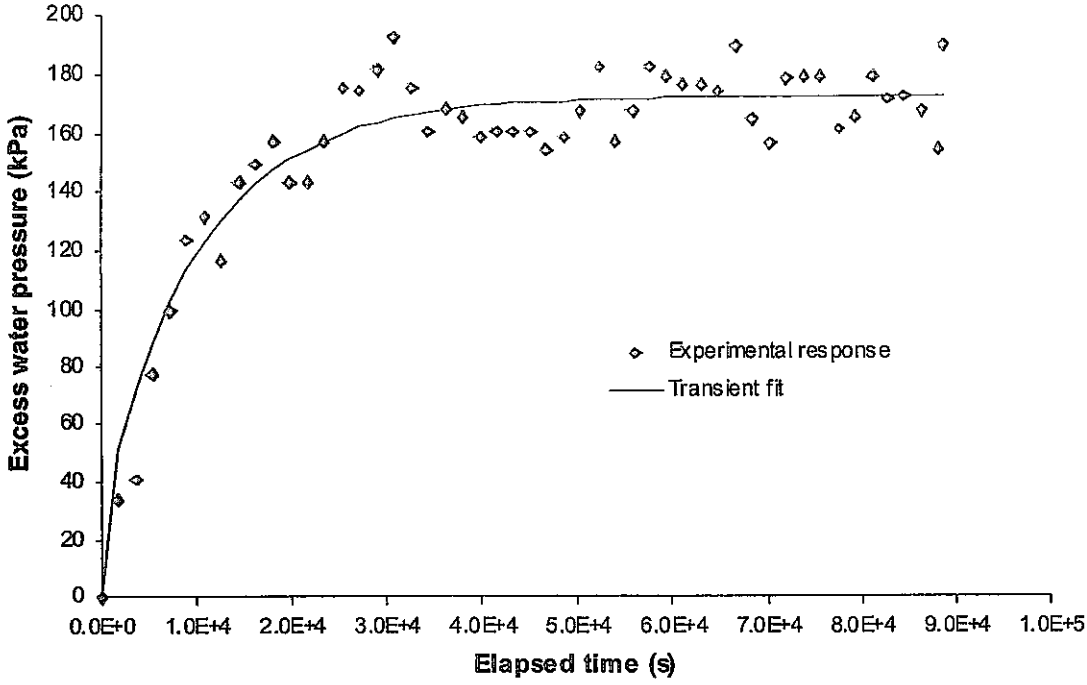

Figure 6 **Transient analysis of excess water pressure (stage 3)**

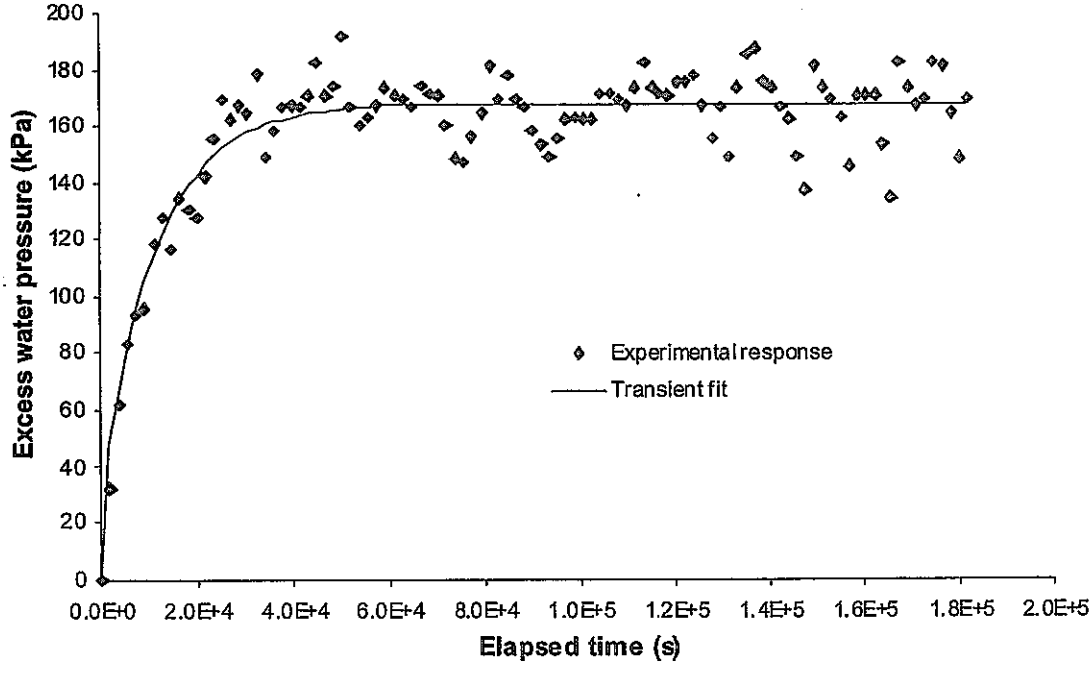

Figure 7 **Transient analysis of excess water pressure (stage 4)**

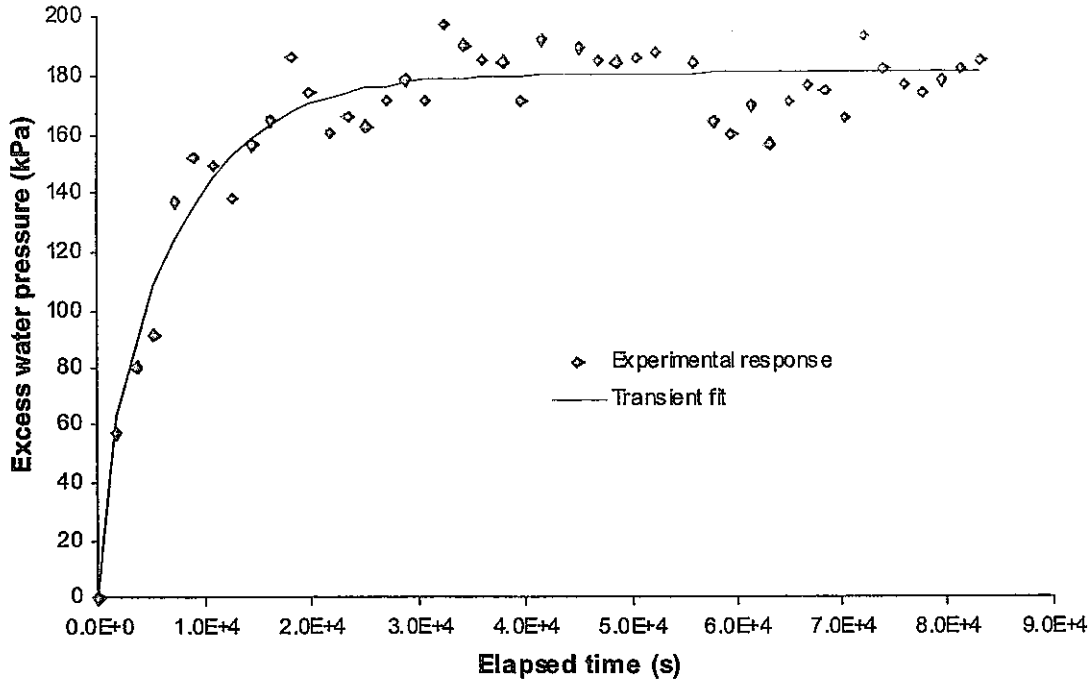

Figure 8 **Transient analysis of excess water pressure (stage 5)**

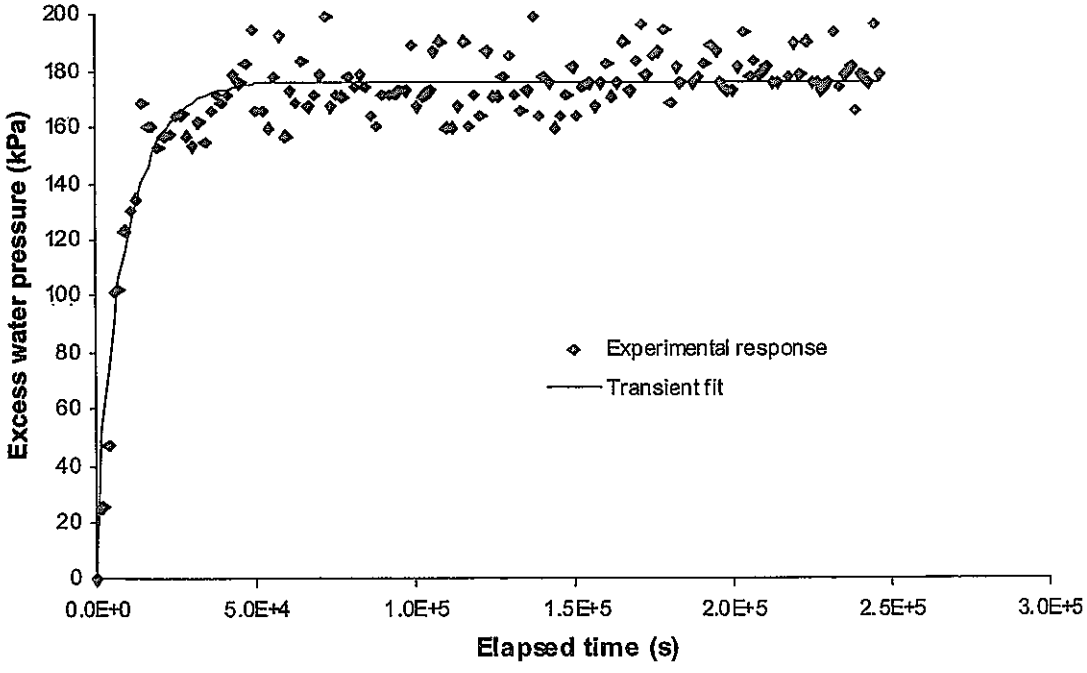

Figure 9 **Transient analysis of excess water pressure (stage 6)**

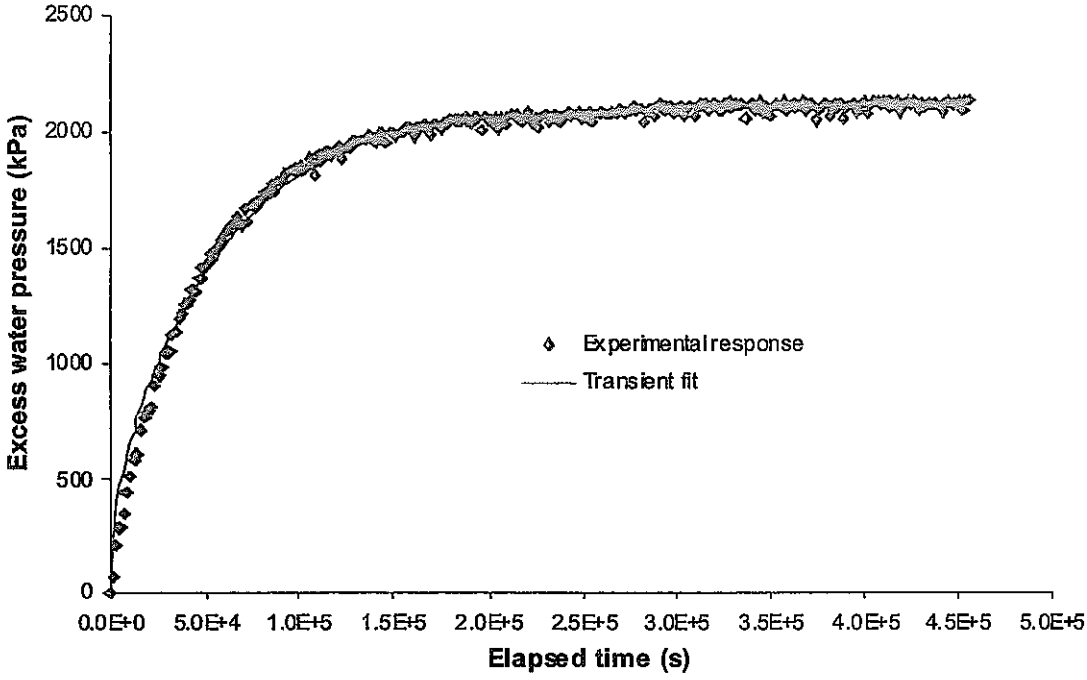

Figure 10 **Transient analysis of excess water pressure (stage 9)**

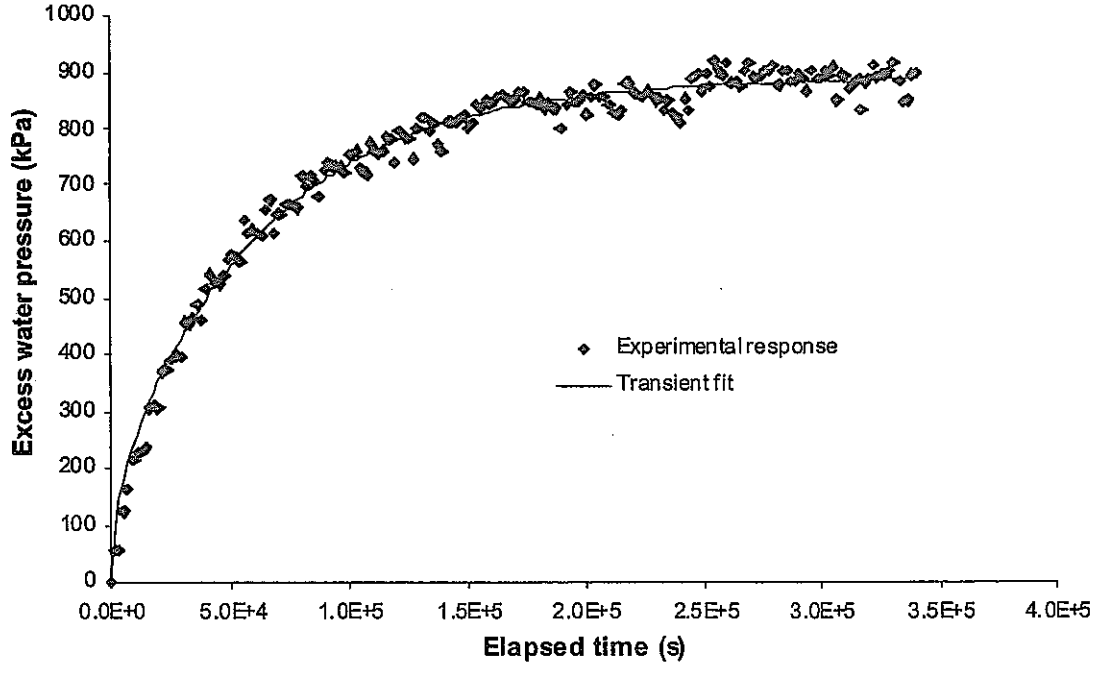

Figure 11 **Transient analysis of excess water pressure (stage 10)**

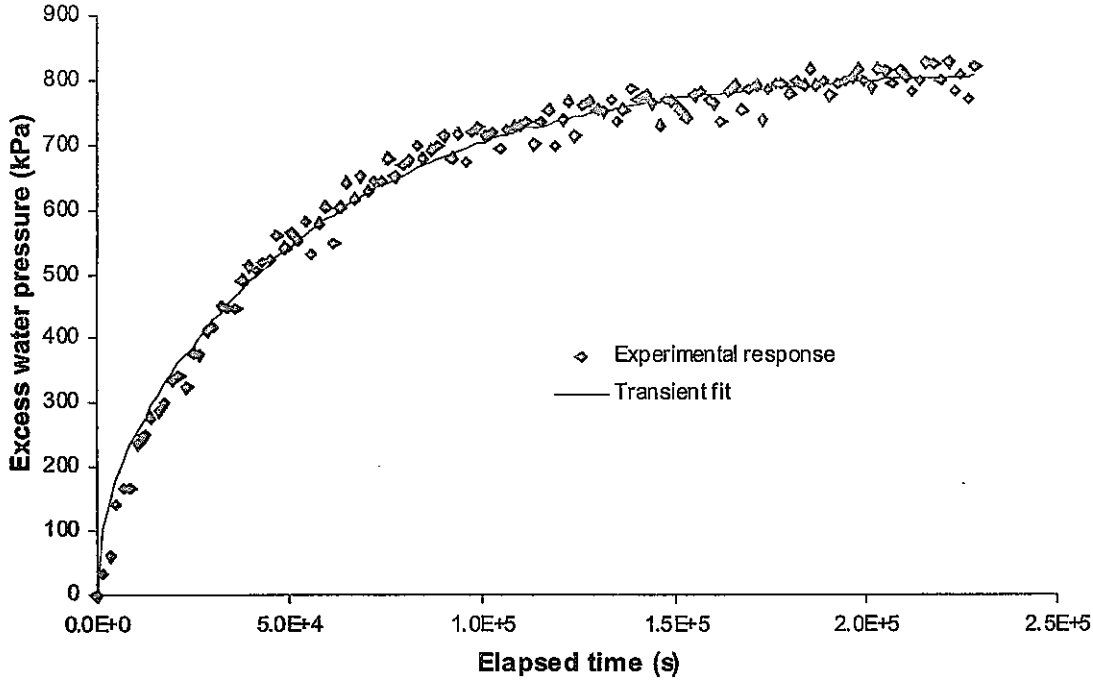

Figure 12 Transient analysis of excess water pressure (stage 11)

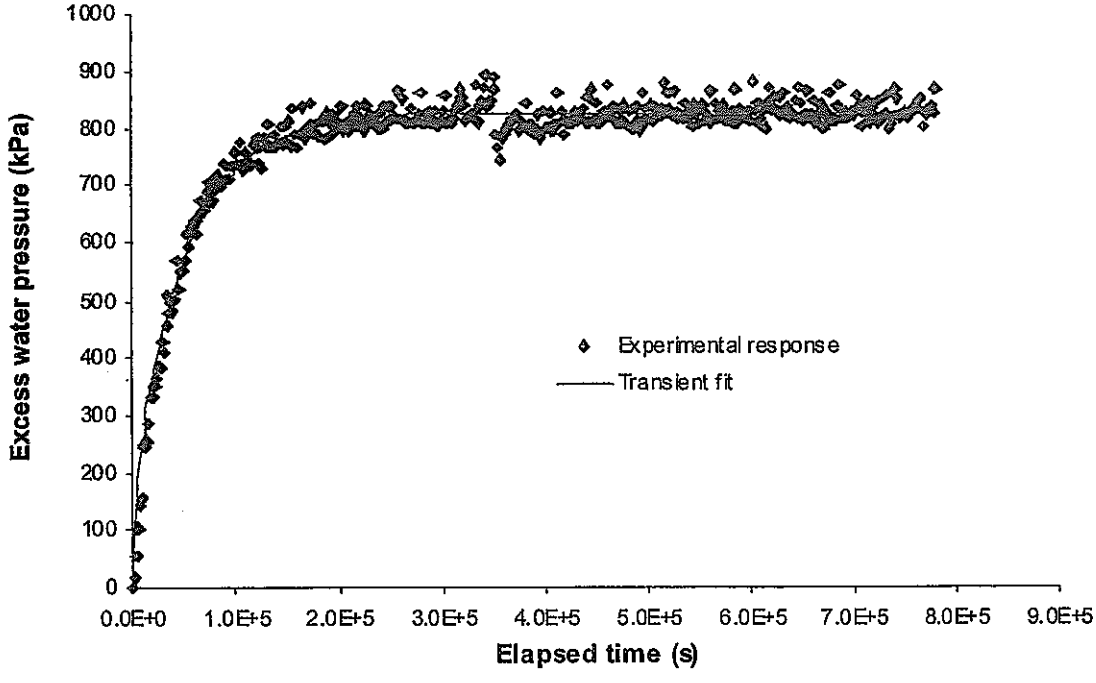

Figure 13 Transient analysis of excess water pressure (stage 12)

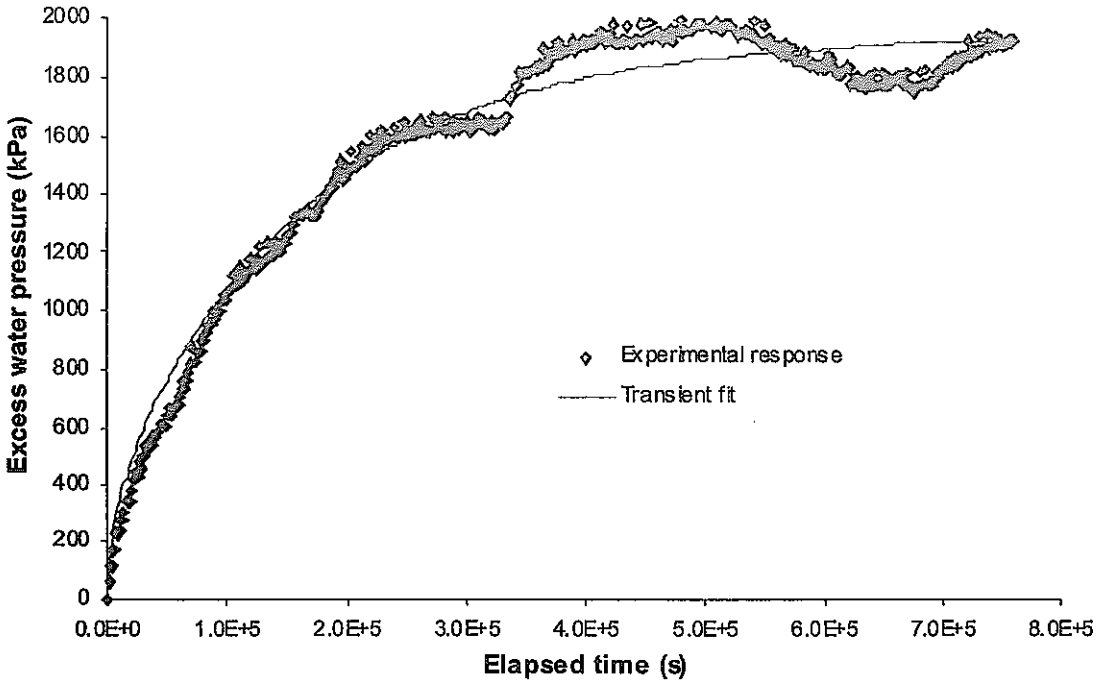

Figure 14 **Transient analysis of excess water pressure (stage 13)**

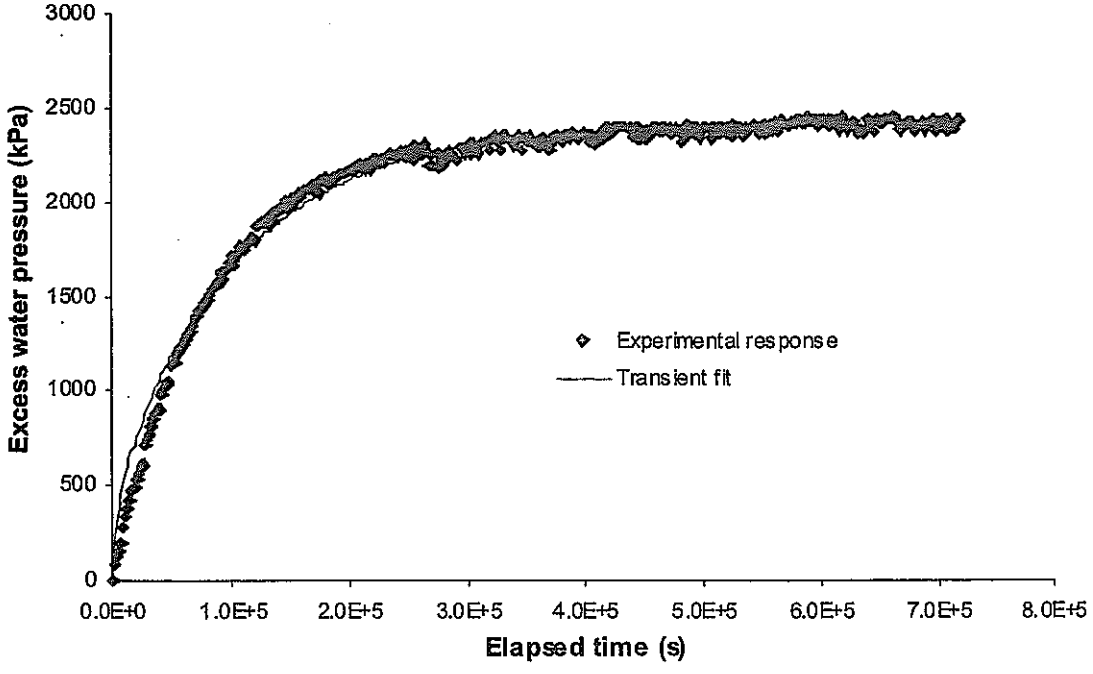

Figure 15 **Transient analysis of excess water pressure (stage 16)**

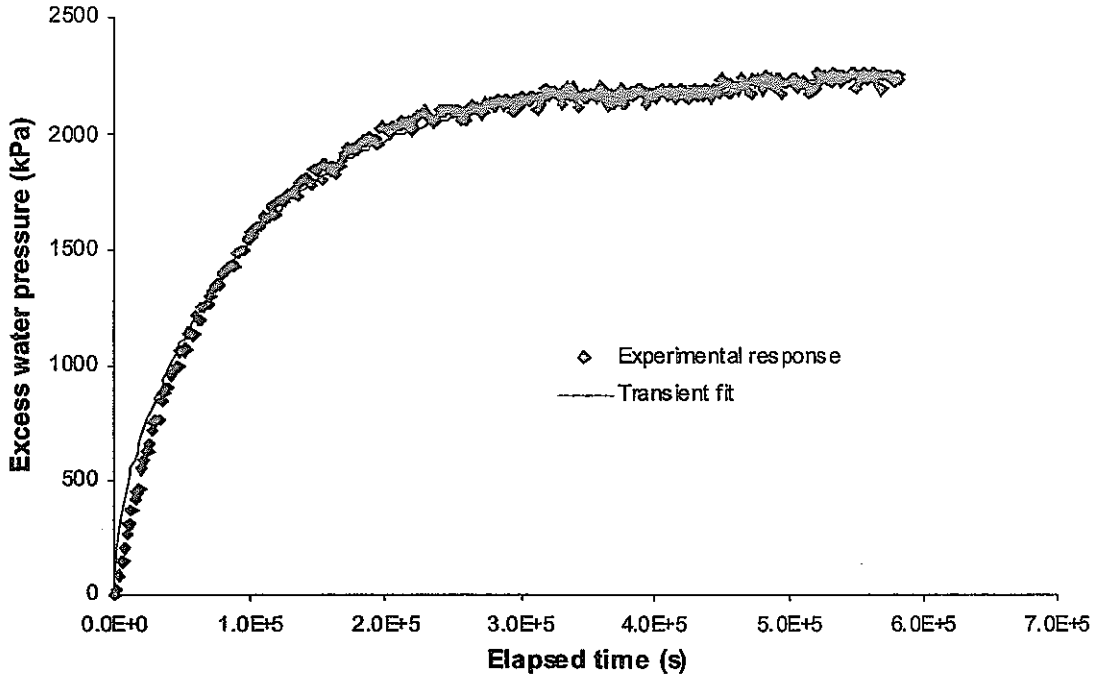

Figure 16 **Transient analysis of excess water pressure (stage 17)**

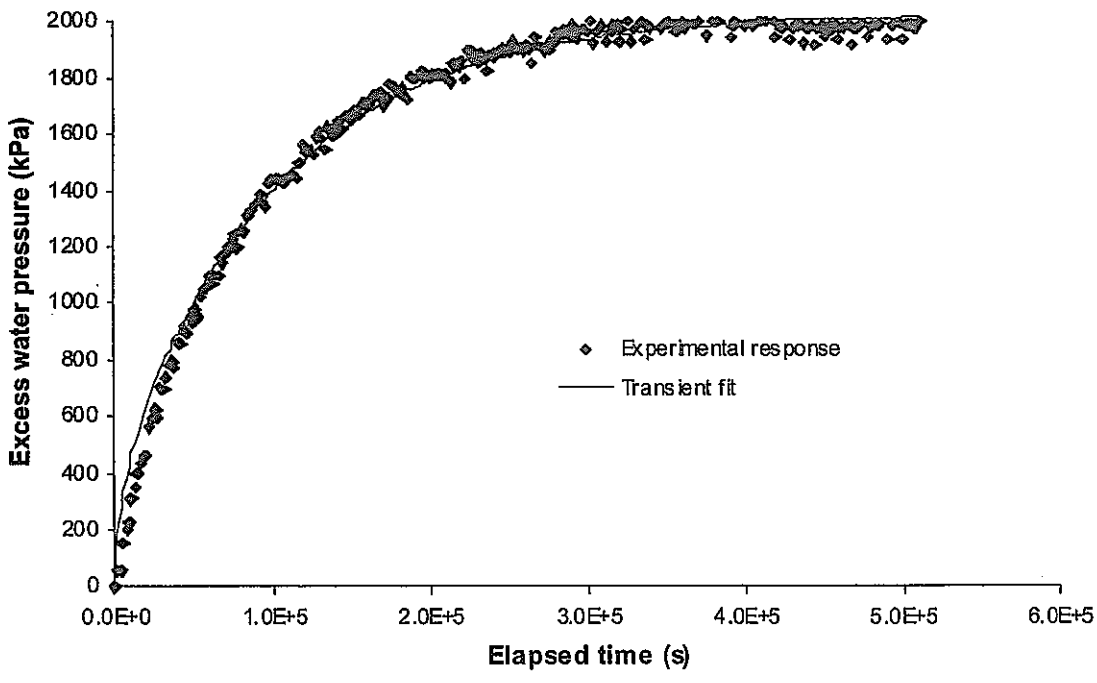

Figure 17 **Transient analysis of excess water pressure (stage 18)**

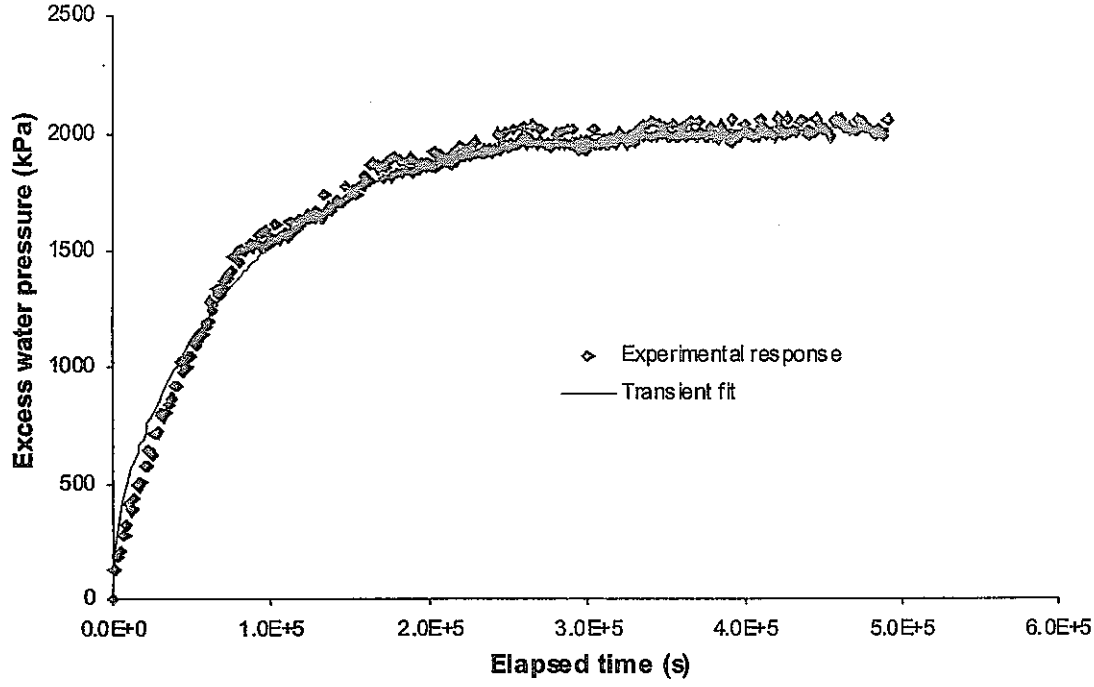

Figure 18 Transient analysis of excess water pressure (stage 19)

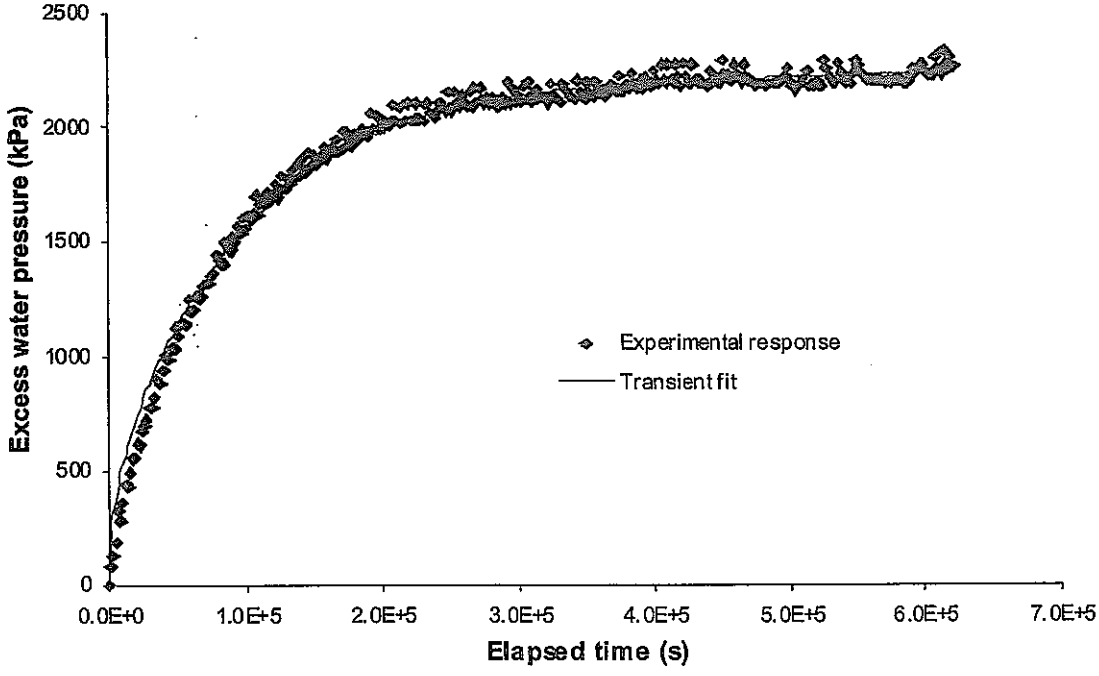

Figure 19 Transient analysis of excess water pressure (stage 20)

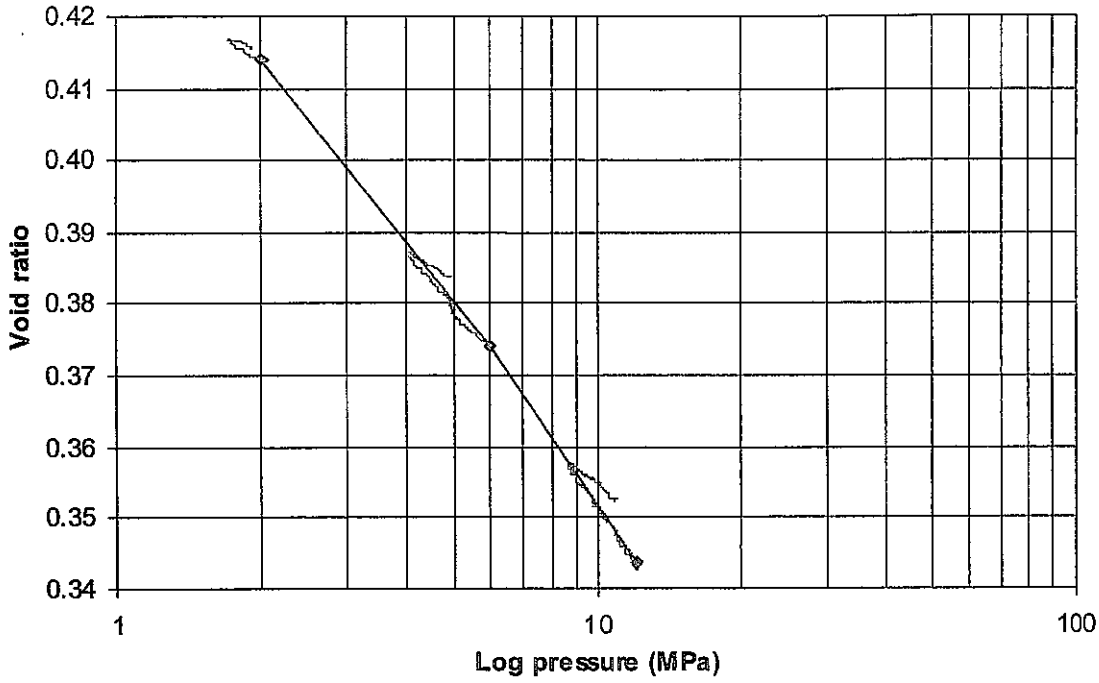

Figure 20 **Void ratio against log effective stress for TFA-1**

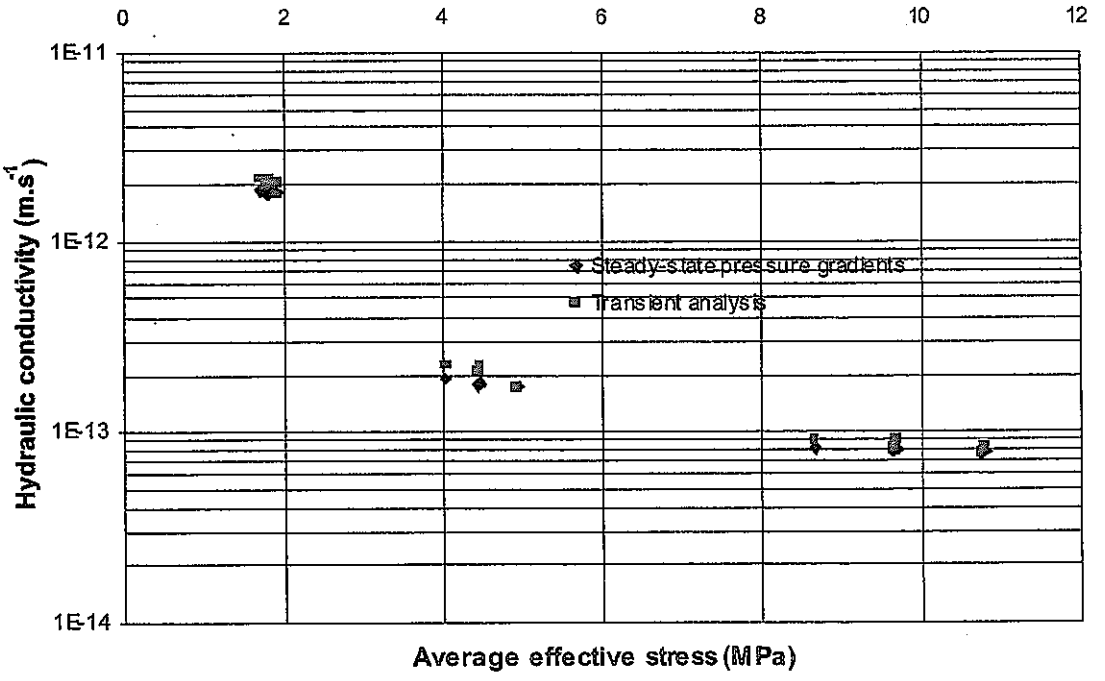

Figure 21 **Hydraulic conductivity against average effective stress**

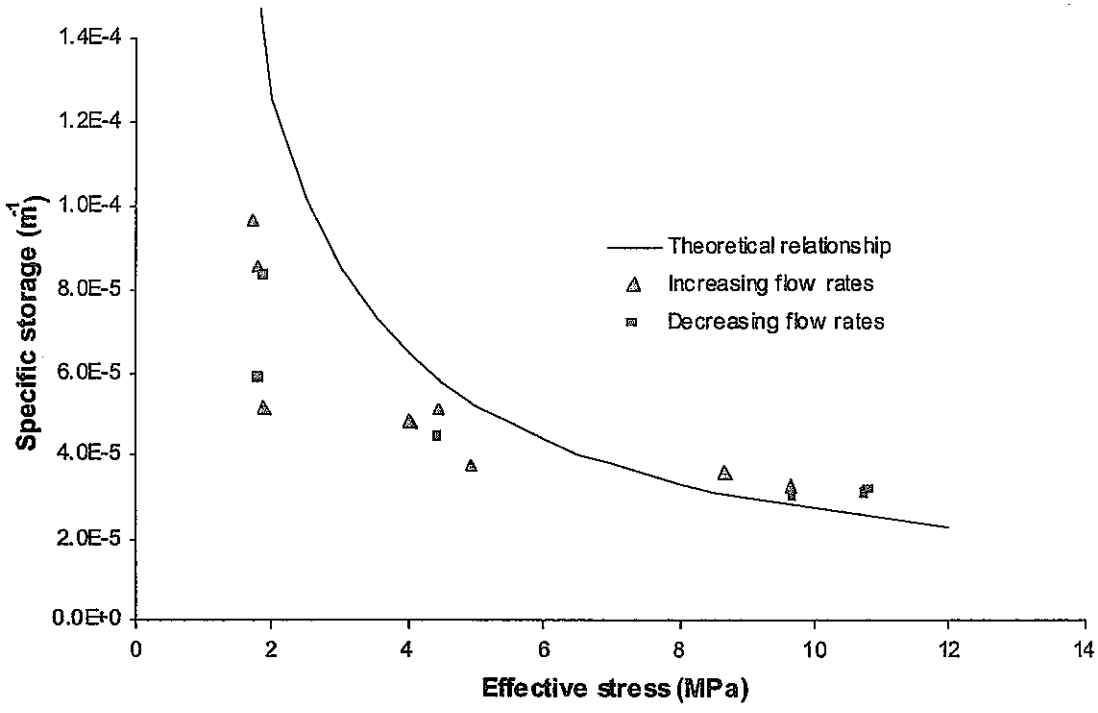

Figure 22 **Specific storage against average effective stress**

APPENDIX 1

Calculation of hydraulic parameters from flow transients

Consider a specimen of length L_s and cross-sectional area A_s with hydraulic head initially everywhere at zero. A fluid flow of Q is initiated at t = 0 into the specimen at the end x = 0 and the response of the hydraulic head at x = 0 is sought as a function of time.

The equation of one-dimensional flow is given by

$$S_s \frac{\partial h}{\partial t} = K \frac{\partial^2 h}{\partial x^2} \qquad \text{(A-1)}$$

where S_s is the specific storage, K is the hydraulic conductivity, and h is the hydraulic head. This equation must be solved subject to the boundary conditions

$$q = \frac{Q}{A_s} = -K \frac{\partial h}{\partial x}\bigg|_{x=0} \qquad \text{(A-2)}$$

and

$$h = 0 \text{ at } x = L_s \qquad \text{(A-3)}$$

To obtain the solution to (A-1), we take its Laplace Transform

$$pS_s \bar{h} = K \frac{\partial^2 \bar{h}}{\partial x^2} \qquad \text{(A-4)}$$

where p is the transform parameter and $\bar{h}$ is the Laplace Transform of the head. The solution to this may be written as

$$\bar{h}(x) = Ae^{(\lambda x)} + Be^{(-\lambda x)} \qquad \text{(A-5)}$$

where A and B are constants to be determined from the boundary conditions and

$$\lambda = \sqrt{\frac{pS_s}{K}} \qquad \text{(A-6)}$$

From the boundary condition in (A-3), we have

$$Ae^{(\lambda L)} + Be^{(-\lambda L)} = 0 \qquad \text{(A-7)}$$

Taking the Laplace Transform of (A-2), we have

$$A\lambda - B\lambda = -\left(\frac{q}{K}\right)\frac{1}{p} \qquad \text{(A-8)}$$

Substituting using (A-7) and re-arranging, we have

$$A = -\left(\frac{q}{K\lambda}\right)\frac{1}{p}\frac{e^{(-\lambda L)}}{\left(e^{(\lambda L)} + e^{(-\lambda L)}\right)} \qquad \text{(A-9)}$$

and

$$B = \left(\frac{q}{K\lambda}\right)\frac{1}{p}\frac{e^{(\lambda L)}}{\left(e^{(\lambda L)} + e^{(-\lambda L)}\right)} \qquad \text{(A-10)}$$

Thus we may write the Laplace Transform of the head at $x = 0$ as

$$\bar{h}(x = 0) = \frac{q}{Kp\lambda}\tanh\left(\lambda L_s\right) \qquad \text{(A-11)}$$

The head at $x = 0$ as a function of time is obtained by numerically inverting the Laplace Transform solution given in Equation A-11 using the method of Talbot (1979). Five parameters are required to define the solution. Three are experimentally determined: Q, A_s and L_s. The remaining two are the material properties that the test is designed to determine (i.e. K and S_s). In order to estimate the values of these parameters, a general nonlinear least squares fitting routine was used to minimise the differences between the calculated curves and the measured head data.